Solar Energy 188 (2019) 185–189

Contents lists available at ScienceDirect

Solar Energy

journal homepage: www.elsevier.com/locate/solener

A two-parameter aiming strategy to reduce and flatten the flux map in solar power tower plants

Francisco J. Collado*, Jesus Guallar

Department of Mechanical Engineering, EINA, Universidad de Zaragoza, María de Luna 3, 50018 Zaragoza, Spain

ARTICLE INFO

Keywords:
Solar power tower plants
Peak heat flux
Aiming strategy
Flattened heat flux profiles

ABSTRACT

In surrounding solar power tower plants, the collector field is designed with all the heliostats pointing to the cylindrical receiver equator to obtain maximum intercept. However, in commercial plants, the addition of thousands of energy spots at the same receiver level causes an excessively high peak heat flux of about 2 MW/m^2. Therefore, this peak flux should be almost halved to avoid receiver problems due to creep and fatigue effects. The single-parameter aiming strategy (Vant-Hull, 2002) has already shown its ability to divide this high peak flux into two lower peaks; it consists in moving the hot spots up and down from the equator, in alternative heliostat rows, to create symmetric flux maps although they are clearly not very homogeneously distributed along the receiver height. In this work, a slight variation of the single-parameter aim strategy, simply proposing two aim parameters, has been successfully tested for a commercial solar power tower plant with a regular layout. The new two-parameter aiming strategy achieves not only reasonable peak flux values, but also an acceptably flattened flux profile and a slight reduction in spillage compared with the single-parameter strategy.

1. Introduction

Current commercial solar power tower plants (≥100 MWe) are surrounded by a heliostat field that concentrates direct radiation onto an external cylindrical receiver atop the central tower. For maximum intercept, which is the fraction of the reflected sunlight hitting the receiver, all the heliostats should be aimed towards the cylindrical receiver equator. However, the cumulative effect of thousands of heliostat energy spots on the same receiver surface level causes high peak fluxes, around 2 MW/m^2 (Relloso and Gutiérrez, 2016). These fluxes are excessive due to creep and fatigue effects throughout the lifetime of the thermal cycles (Falcone, 1986). Therefore, an aiming strategy spreading energy images along the receiver height should be defined to drastically reduce these flux levels.

This spread should not excessively increase the fraction of reflected sunlight failing to strike the receiver, or 'spillage'. Moreover, Logie et al. (2018) show that reducing peak heat flux and obtaining more homogeneous flux distributions are both required to control peak thermal stress.

In conclusion, optimising of the aim point distribution of the heliostat field on the receiver would seek to lower the peak flux significantly, to flatten the flux distribution, and, at the same time, avoid excessive energy loss due to spillage increase.

Given the large number of mirrors in the collector field of commercial plants, optimising heliostat aim point combinations is a complex mathematical problem (Belhomme et al., 2014; Flesch et al., 2017; Conroy et al., 2018). However, a much simpler aiming strategy has recently been put into practice by Sanchez-Gonzalez and Santana (2015), Sanchez-Gonzalez et al. (2017) following a single-parameter strategy, first suggested by Vant-Hull (2002), for the entire heliostat field. In this strategy, heliostat aim points have been moved from the equator and are now located taking as reference the upper or the lower receiver edge, in alternate heliostat rows to obtain symmetric flux maps. The distance of the new aim point to the edge is equal to the product of the heliostat beam radius by a single parameter k, which controls the aiming process for the entire field.

The same aiming strategy has been also used by Collado and Guallar (2018) to halve the peak heat flux in a commercial solar power plant (Noor III-like, 7400 heliostats, 150 MWe). However, this single-parameter aiming strategy produces a rather irregular flux profile with two peaks along the receiver height, which is clearly not convenient for peak thermal stress.

Finally, Sanchez-Gonzalez et al. (2018) have recently presented a more sophisticated aiming strategy, similar to that of Astolfi et al. (2017), intended to produce more uniform flux profiles. The heliostat field is divided in sectors according to their respective target receiver

* Corresponding author.
E-mail address: fjk@unizar.es (F.J. Collado).

https://doi.org/10.1016/j.solener.2019.06.001
Received 24 January 2019; Received in revised form 9 May 2019; Accepted 2 June 2019

panels (18 panels for the case study chosen) and then their specific parameters k_i are deterministically selected seeking the flattest flux vertical profiles in each receiver panel.

In this technical note, a slight modification of the Vant-Hull (2002) single-parameter aiming strategy is proposed to improve the uniformity of the heat flux profile on the receiver. The new proposed strategy works with two parameters for the whole field.

The recently optimised surrounding radially staggered Noor III-like plant (Collado and Guallar, 2018) is used here as case study to check the new strategy. The main optimisation parameters of that optimisation are listed in (Collado and Guallar, 2018). The collector field has a 'regular' layout with three zones, a tower optical height (THT) of 250 m, and a cylindric receiver with a diameter of 17 m (RD) and an a height of 20.4 m (RH). Appendix A (electronic pdf file) includes a brief outlook on how a 'regular' layout is generated and how the three zones are defined.

The flux is simulated with the HFLCAL model from DLR (Schmitz et al., 2006; Schwarzbölz et al., 2009), which uses a circular normal (Gaussian) distribution of the energy reflected by the heliostat, and it also assumes that all heliostats have well-canted concentrating facets of spherical curvature. The suggested aiming modification is tested using the flux map procedure presented in Collado and Guallar (2018).

Finally, three representative days of the typical meteorological year (TMY) at the Plataforma Solar de Almería (PSA) are checked, i.e. spring equinox, summer solstice and winter solstice. After a brief outline of the Vant-Hull (2002) single-parameter aiming strategy, the suggested aiming modification is explained and tested, and some conclusions are drawn.

2. Vant-Hull (2002) single-parameter aiming strategy

As we have already advanced above, to reduce peak flux, the single-parameter procedure moves the heliostat aim point away from the receiver equator in a vertical direction along the cylinder surface, without modifying its azimuth. The aim point of any mirror will be the centre of its flus density spot.

Since spillage has to be considered in spreading the hot spots along the receiver, Vant-Hull (2002) proposes that these circular spots, projected onto the receiver, should be tangent to either the upper or the lower cylinder edges, in alternate heliostat rows, to produce symmetric flux maps.

Therefore, the vertical position of any heliostat aim point from the receiver edge would be the radius of its projected beam cone. As the beam cone has a circular normal distribution, it is necessary to define its radius through its effective standard deviation.

The key point of the Vant-Hull aiming strategy is to modulate the radius of the circular energy spots multiplying their effective standard deviation by a parameter k, that ranges between 0 and 5 (Collado and Guallar, 2018).

Therefore, the actual beam radius at the image plane would be

$$(rk)_{image} = k\sigma_{HF}, \tag{1}$$

where σ_{HF} (m) is the effective deviation of the convolution of the four Gaussian error functions considered. Full details about σ_{HF} can be found in Collado and Guallar (2018). After projecting onto the receiver vertical, the modulated beam radius $rk(m)$ on the receiver surface, see Fig. 1, becomes

$$rk = k\sigma_{HF}/sin\varepsilon_T, \tag{2}$$

where ε_T is the elevation angle, from the zenith, of the heliostat's central reflected ray.

Obviously, the larger k is, the larger the effective beam radius is, Eq. (2). Thus, as any circular spot has to be tangent to the edge, the flux density centre i.e., the aim point, is moved towards the equator (increasing intercept), the limit being the own equator.

For a large surrounding solar power tower plant as Noor III, it has been found (Collado and Guallar, 2018) that, when $k \geq 5$, the increased beam diameter is always higher than the cylindrical receiver height. In this case, the aim point is the cylinder equator and spillage is minimum, although peak flux is maximum.

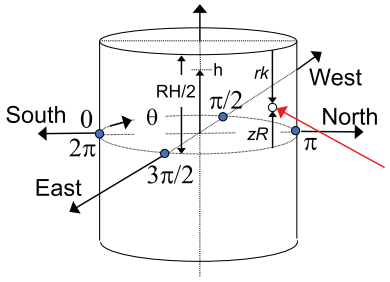

Fig. 1. Coordinates on the cylindrical receiver surface. North hemisphere.

However, by lowering k, the centres of the energy images come closer to the upper or lower edges of the receiver, in alternate heliostat rows. Hence, the original whole flux map around equator ($k = 5.0$) is approximately divided into two spots by decreasing k to about $1.8 - 2$. If we continue lowering k, these two spots gradually move further away from equator, and their respective peak fluxes drop. The flux map is flattened, (Sanchez-Gonzalez et al., 2017) but the spillage also increases.

Finally, to highlight that Vant-Hull aiming strategy has more subtle and significant points, in particular, how sharp flux at the top and the bottom of the receiver are decreased to a level defined by the allowable flux density on the end shields. More details can be found in Vant-Hull and Pitman (1990), Vant-Hull et al. (1996).

2.1. Location of the aim points from the receiver equator

The Vant-Hull strategy, explained above, is also followed in Collado and Guallar (2018). Consequently, the vertical distance from any heliostat aim point to the receiver edge is the radius of its projected beam cone (rk), see Eq. (2). This new aim point has the same azimuth as the original equator aiming strategy.

However, here, for the sake of convenience, the location of this same aim point is merely referenced to the receiver equator, $zR(m)$. Therefore, at first instance, and for upwards equator aiming, $RH/2 = rk + zR$, see Fig. 1. Although the aiming procedure for a heliostat in any row previously would have to test whether the projection of the working beam radius rk was greater than half the receiver height i.e., $rk \geq RH/2$; in this case, the heliostat would be pointed towards the receiver equator ($zR = 0.0$) to minimise spillage. Otherwise, for odd rows (upwards equator)

$$zR = \frac{RH}{2} - rk, \tag{3}$$

whereas for even rows (downwards equator)

$$zR = -\frac{RH}{2} + rk. \tag{4}$$

3. New two-parameter aiming strategy

For a Noor III-like plant, the Vant-Hull (2002) single parameter aim procedure has been successfully used elsewhere (Collado and Guallar, 2018) to almost halve the peak heat flux i.e. from 2.04 MW/m^2 with $k = 5$ (equator aiming) to 1.08 MW/m^2 using $k = 1.8$ at summer solstice noon. Note that the same value of k has been used for all the heliostats in the field.

For easier understanding of the figures shown in this study, Fig. 1 shows the receiver surface coordinates. A point on the receiver surface is located by its vertical height h (from the equator plane) and its

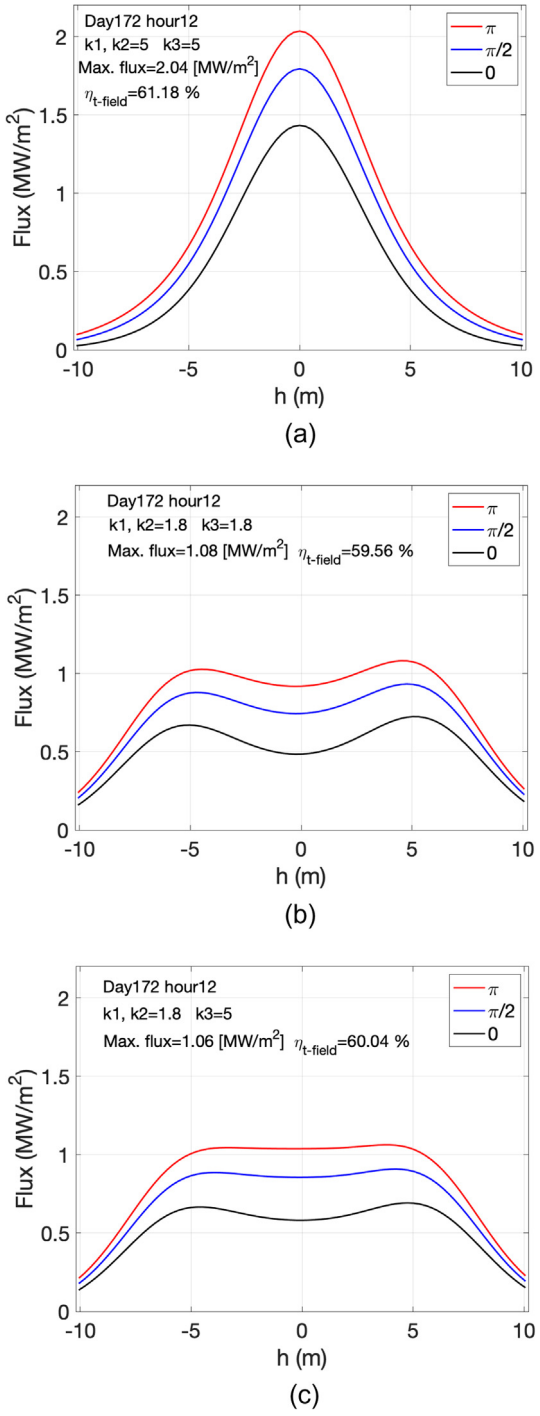

Fig. 2. Flux profiles on the receiver on the summer solstice noon. (a) Aiming factors ($k_1 = k_2 = k_3 = 5.0$). (b) Aiming factors ($k_1 = k_2 = k_3 = 1.8$). (c) Aiming factors ($k_1 = k_2 = 1.8$, $k_3 = 5.0$).

receiver azimuth θ (origin in the South, positive towards the West). In the northern hemisphere, the maximum flux is located on the North side of the receiver. For example, at noon, it would be around π, see Fig. 1.

Thus, Fig. 2a shows the huge flux peaks in the profiles on the receiver surface along the receiver height, for different azimuths, at summer solstice noon, for $k = 5$ (equator aim), whereas Fig. 2b presents the drastic drop in the profiles using the Vant-Hull single-parameter aiming strategy with $k = 1.8$ at the same instant of time. Although the peak heat flux has been practically halved by dispersing the aim points from equator, the resulting flux profile is not homogeneous along the receiver height presenting two clear peaks: one above the equator and one below it.

From Fig. 2a–b, it is clear that lowering k from $k = 5$, $\eta_{t-field} = 61.18\%$, to $k = 1.8$, $\eta_{t-field} = 59.56\%$, causes an efficiency reduction of 1.62 points. Clearly, there is a trade-off between the resulting peak flux and the spillage i.e., the higher the peak flux, the lower the spillage, i.e. the higher the instantaneous field efficiency $\eta_{t-field}$.

In conclusion, to avoid undesired thermal stresses and extend the receiver service life (Logie et al., 2018; Sanchez-Gonzalez et al., 2018), we should somehow flatten this gap and these peaks in the flux profile while trying to limit the spillage increase and hold the peak flux below reasonable limits.

The analysis of Fig. 2b could suggest filling in the central gap between the two peaks with heat flux from both peaks, which would, in turn, be reduced. One way to do this is to redirect the heliostats of zone 3 towards the equator again ($k_3 = 5$) while heliostat aim points of zones 1 and 2 are moved upwards and downwards from equator, in alternate rows, following ($k_1 = k_2 \leq 5$). Again, see electronic Appendix A for the definition of these three zones in a 'regular' field.

Indeed, this two-parameter aiming strategy would be equivalent to one of the suggestions of Vant-Hull (2002) on how to avoid 'shoulders', see Fig. 2b; specifically, returning a fraction of the beams back to aim at the equator. In this study, this beam fraction would come from the zone 3 heliostats, which is the furthest zone from the tower.

Applying this new two-parameter aiming strategy for the analysed plant, at the same instant of time as above, with $k_1 = k_2 = 1.8$, and $k_3 = 5$, achieves an acceptable flattening of the vertical flux profiles for the whole cylinder, see Fig. 2c. Nevertheless, the flattening effect is more pronounced at higher levels of flux, θ = π, whereas, for θ = 0, with lower flux, the flattening is not so homogeneous. For this new two-parameter aim strategy, Fig. 3 shows the flux map on the unfold cylindrical receiver surface.

Regarding the intercept or spillage, note that the zone 3 redirection towards the equator not only flattens the profile but also increases the $\eta_{t-field}$(60.04%) by reducing the spillage, in comparison with the original single-parameter ($k = 1.8$) strategy ($\eta_{t-field} = 59.56\%$). The reason is that the zone 3 is the furthest one from the tower with the broadest spots as a result. Therefore, the spillage will be very sensitive to small movements of these large images from the equator.

The main objective of this study is to explore relevant couples of parameters ($k_1 = k_2$, k_3), which could flatten the heat flux profiles along three representative days in the year, i.e. spring equinox, summer solstice and winter solstice, for the Noor III-like plant optimized in Collado and Guallar (2018). Three simultaneous objectives are sought with the following ranking order:

(1) To appropriately flatten the vertical flux profiles
(2) The maximum peak flux should be as low as possible and always ≤ 1.15 MW/m^2.
(3) The decrease in $\eta_{t-field}$ from the maximum efficiency (equator aiming) should be $\leq 1\%$.

The second objective is supported by Sener (Relloso and Gutiérrez, 2016), which estimates that the maximum peak allowed by the current tube materials is in the range 1–1.2 MW/m^2. The last objective would establish a reasonable limit for the associated efficiency loss to spread the energy spots and try to flatten the heat flux. Clearly, the ranking order of the objectives could be redefined by economic reasons. For example, if the peak heat flux did not increase excessively and the receiver damage were not high, it could be decided to get higher field efficiencies by lowering $k_1 = k_2$.

4. Results

For a Noor III-like plant (Collado and Guallar, 2018), Table 1 shows

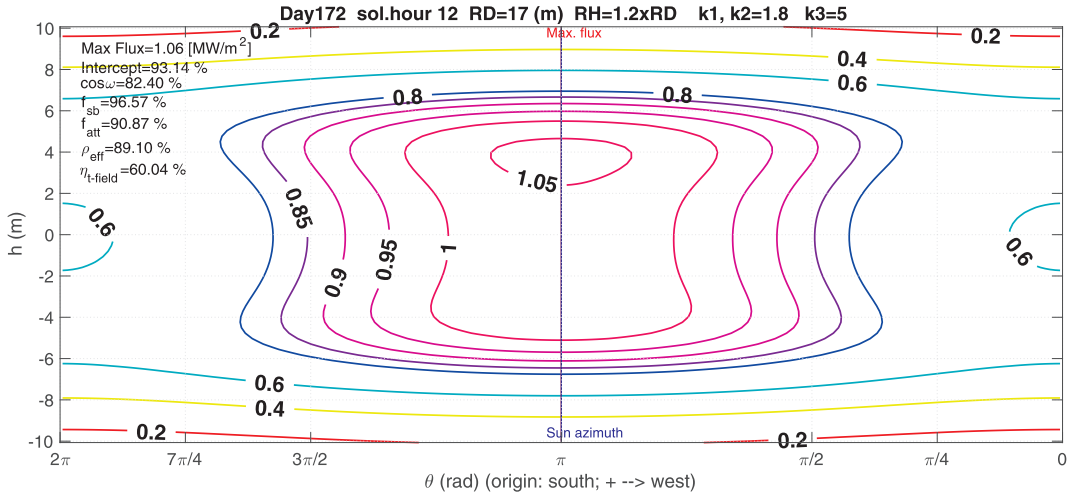

Fig. 3. Flux map on the unfolded cylindrical receiver. ($k_1 = k_2 = 1.8$, $k_3 = 5.0$).

Table 1
Two-parameter aiming strategy for a Noor III-like collector field in Almeria (PSA).

Day	Solar hour	DNI (kW/m^2)	[$k_1 = k_2$, k_3]	Peak flux (MW/m^2)	$\eta_{t\text{-field}}$ (%)	$\Delta\eta_{t\text{-field}}$ (%)
Spring equinox (81)	8.0	0.655	[5.0]	1.36	50.87	0.0
			[2.4]	0.87	50.54	0.33
	10.0	0.878	[5]	1.98	58.57	0.0
			[1.8, 5.0]	1.04	57.36	1.21
			[1.9, 5.0]	1.07	57.59	0.98
			[2.0, 5.0]	1.10	57.78	0.79
	12.0	0.918	[5.0]	2.07	60.27	0.0
			[1.8, 5.0]	1.08	59.08	1.19
			[1.9, 5.0]	1.11	59.31	0.96
			[2.0, 5.0]	1.15	59.50	0.77
Summer solstice (172)	7.0	0.693	[5.0]	1.39	50.59	0.0
			[2.4]	0.88	50.25	0.34
	8.0	0.835	[5.0]	1.82	55.74	0.0
			[1.8, 5.0]	0.94	54.52	1.22
			[1.9, 5.0]	0.96	54.75	0.99
			[2.0, 5.0]	0.99	54.94	0.8
	10.0	0.939	[5]	2.04	60.14	0.0
			[1.8, 5.0]	1.06	58.97	1.17
			[1.9, 5.0]	1.09	59.20	0.94
			[2.0, 5.0]	1.12	59.39	0.75
	12.0	0.96	[5.0]	2.04	61.18	0.0
			[1.8, 5.0]	1.06	60.04	1.14
			[1.9, 5.0]	1.09	60.27	0.91
			[2.0, 5.0]	1.12	60.46	0.72
Winter solstice (345)	9.0	0.489	[5.0]	0.9	45.06	0.0
			[2.4]	0.60	44.76	0.30
	10.0	0.653	[5]	1.40	52.02	0.0
			[1.8, 5.0]	0.76	50.89	1.13
			[1.9, 5.0]	0.78	51.09	0.93
			[2.0, 5.0]	0.80	51.26	0.76
	12.0	0.753	[5.0]	1.68	55.72	0.0
			[1.8, 5.0]	0.89	54.52	1.20
			[1.9, 5.0]	0.92	54.74	0.98
			[2.0, 5.0]	0.95	54.92	0.80

In bold, the selected two parameters (only one if they are equal).

the options checked for the new two-parameter aiming strategy at different instants of time during spring equinox (day 81), summer solstice (day 172) and winter solstice (day 345); the resulting peak heat flux, the field efficiency, and reduction of efficiency regarding maximum efficiency are also shown. For the sake of comparison, at every instant of time, the first row shows the results with a single-parameter equatorial aiming strategy (k = 5.0), i.e. the highest peak flux but also the maximum intercept and, therefore, the maximum instantaneous field efficiency $\eta_{t-field,max}$.

For any two-parameter aiming strategy, the field efficiency $\eta_{t-field}$ is lower than the maximum $\eta_{t-field,max}$. Thus, we can define the reduction of the instantaneous field efficiency $\Delta\eta_{t-field}$, the last column in Table 1, as $\Delta\eta_{t-field} = \eta_{t-field,max} - \eta_{t-field}$.

First, for the large majority of the time instants considered, the selected two parameters (in bold) of the new aiming strategy are the same and equal to ($k_1 = k_2 = 1.9$, $k_3 = 5$). The selection of these parameters is based on the above ranking order.

For instance, on spring equinox at solar hour 10.0, equator aiming ($k = 5$) causes a very high peak heat flux, 1.98 MW/m^2, but the new aiming strategy ($k_1 = k_2 = 1.8$, $k_3 = 5$) drastically reduces the peak flux to 1.04 MW/m^2. However, the efficiency decrease $\Delta\eta_{t-field}$ is 1.21% (higher than 1%). Consequently, to maintain the efficiency reduction $\leq$1%, the spot spread should be reduced, so that the first parameter is slightly increased ($k_1 = k_2 = 1.9$, $k_3 = 5$). Now, $\Delta\eta_{t-field} = 0.98\%$ is within the limit although its corresponding peak flux, 1.07 MW/m^2, becomes slightly higher than before. The related heat flux profiles along the receiver height can be seen in Fig. 4.

Note that the $\eta_{t-field}$ could be further improved by increasing parameter k for zones 1 and 2, ($k_1 = k_2 = 2.0$, $k_3 = 5$) but the peak flux

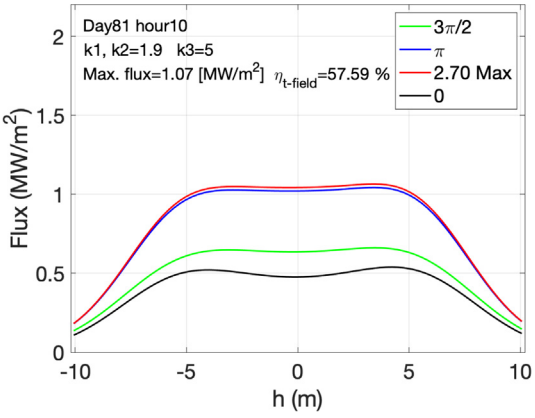

Fig. 4. Flux profiles on the receiver on the spring equinox at 10 solar hour ($k_1 = k_2 = 1.9$, $k_3 = 5.0$).

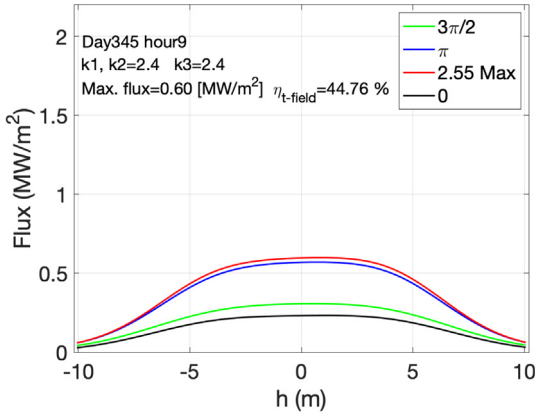

Fig. 5. Flux profiles on the receiver on the winter solstice at 9 solar hour ($k_1 = k_2 = k_3 = 2.4$).

would increase to 1.10 MW/m^2. As the proposed rule is to reduce the peak flux as much as possible, provided that $\Delta\eta_{t-field} \leq 1\%$, the aim strategy ($k_1 = k_2 = 1.9$, k_3=5) would be chosen.

Finally, during the first hours of the day, or the evening hours, with low sun elevations and generally low solar direct normal intensity (DNI), the single-parameter aim strategy suffices to achieve the three proposed objectives. The value chosen was ($k_1 = k_2 = k_3$=2.4). Fig. 5 shows the heat flux profiles with this single-parameter aiming strategy for winter solstice at solar hour 9.0.

5. Conclusions

In surrounding commercial solar power plants, an aiming strategy spreading the mirror focal spots along the height of the cylindrical receiver is needed to avoid excessively high peak fluxes (Vant-Hull, 2002). The spillage increase caused by the aiming strategy should be controlled. Heat flux profiles also need to be conveniently flattened to reduce peak thermal stress (Logie et al., 2018).

In the single-parameter aiming point strategy (Vant-Hull, 2002), only one parameter k controls the aiming strategy for the entire field. For a Noor III-like plant with 7400 heliostats and 150 MWe of nominal power, this quite simple procedure has already proven its ability (Collado and Guallar, 2018) to almost halve the peak heat flux, without an excessive loss of efficiency, with a $k = 1.8$. However, it has also been verified that, in general, this single-parameter aiming strategy causes two heat-flux peaks, up and down the equator, respectively. Therefore, such an irregular flux profile should be flattened in some manner.

Here, the use of two parameters for a Noor III-like 'regular' layout field with three zones is suggested, see electronic Appendix A. For the zones 1 and 2, which are the closest to the tower and have the most compact spots, we would use the same parameter, i.e. $k_1 = k_2$ 1.9, whereas for zone 3, which is the furthest from the tower and has the broadest images, we would set $k_3 = 5.0$, which is equivalent to equatorial aiming. This slight modification of the Vant-Hull (2002) strategy achieves not only a bearable peak heat flux but also an acceptable flux flattening, as well as an improvement of the efficiency field by reducing the spillage compared to the single-parameter aiming strategy.

Finally, this aim strategy ($k_1 = k_2$ 1.9, $k_3 = 5.0$) is the same for the vast majority of the instants of time checked with the exception of early morning or late evening. For these last cases, the original single-parameter aiming strategy produces an acceptable flattened profile on its own with $k = 2.4$.

Acknowledgments

The authors want to thank the Spanish Minister of Science and Innovation and the European Regional Development Fund for the funding of this research through the research project ENE2015-67518-R.

Appendix A. Supplementary data

Supplementary data to this article can be found online at https://doi.org/10.1016/j.solener.2019.06.001.

References

Astolfi, M., Binotti, M., Mazzola, S., Zanellato, L., Manzolini, G., 2017. Heliostat aiming point optimization for external tower receiver. Sol. Energy 157, 1114–1129.
Belhomme, B., Pitz-Paal, R., Schwarzbözl, P., 2014. Optimization of heliostat aim point selection for central receiver systems based on the ant colony optimization metaheuristic. J. Sol. Energy Eng. Trans. ASME 136, 011005.
Collado, F.J., Guallar, J., 2018. Fast and reliable flux map on cylindrical receivers. Sol. Energy 169, 556–564.
Conroy, T., Collins, M.N., Fisher, J., Grimes, R., 2018. Thermal and mechanical analysis of a sodium-cooled solar receiver operating under a novel heliostat aiming point strategy. App. Energy 230, 590–614.
Falcone, P.K., 1986. A Handbook for Solar Central Receiver Design. SAND86-8009.
Flesch, R., Frantz, C., Maldonado Quinto, D., Schwarzbözl, P., 2017. Towards an optimal aiming for molten salt power towers. Sol. Energy 155, 1273–1281.
Logie, W.R., Pye, J.D., Coventry, J., 2018. Thermoelastic stress in concentrating solar receiver tubes: a retrospect on stress analysis methodology, and comparison of salt and sodium. Sol. Energy 160, 368–379.
Relloso, S., Gutiérrez, Y., 2016. SENER molten salt tower technology. Ouarzazate NOOR III case. In: Al Obaidli, A. (Ed.), SolarPACES 2016, AIP Conference Proceedings 1850, No. 030041.
Sanchez-Gonzalez, A., Santana, D., 2015. Solar flux distribution on central receivers: a projection method from analytic function. Renew. Energy 74, 576–587.
Sanchez-Gonzalez, A., Rodriguez-Sanchez, M.R., Santana, D., 2017. Aiming strategy model based on allowable flux densities for molten salt central receivers. Sol. Energy 157, 1130–1144.
Sanchez-Gonzalez, A., Rodriguez-Sanchez, M.R., Santana, D., 2018. Aiming factor to flatten the flux distribution on cylindrical receivers. Energy 153, 113–125.
Schmitz, M., Schwarzbölz, P., Buck, R., Pitz-Paal, R., 2006. Assessment of the potential improvement due to multiple apertures in central receiver systems with secondary concentrators. Sol. Energy. 80, 111–120.
Schwarzbölz, P., Schmitz, M., Pitz-Paal, R., 2009. Visual HFLCAL–a software tool for layout and optimization of heliostat fields. Proceedings SolarPACES, Berlin, Germany.
Vant-Hull, L.L., Pitman, C.L., 1990. Static and dynamic response of a heliostat field to flux density limitations on a central receiver. Proceedings of 1990 ASME Int. Solar Engineering Conf., Miami, USA.
Vant-Hull, L.L., Izygon, M.E., Pitman, C.L., 1996. Real time computation and control of solar flux density on a central receiver (Solar Two-protection against excess flux density). In: Campbell-Howe, R., Wilkins-Crowder, B. (Eds.), Proceedings of the 1996 American Solar Energy Soc. Annual Conf., Asheville, USA, pp. 88–94.
Vant-Hull, L.L., 2002. The role of "allowable flux density" in the design and operation of molten-salt solar central receivers. J. Sol. Energy Eng. Trans. ASME 124 (2), 165–169.